https://doi.org/10.5194/egusphere-2026-3971
Preprint. Discussion started: 20 August 2026

Temperature uncertainty characterisation of the FrESH droplet-freezing assay

Germán Perez Fogwill and André Welti

Finnish Meteorological Institute, Helsinki, Finland

Correspondence: Germán Perez Fogwill (german.perez-fogwill@fmi.fi)

Abstract.

Reliable offline measurements of ice-nucleating particles (INPs) with droplet-freezing assays require accurate assignment of droplet temperature. We present FrESH (Freezing Experiment Setup Helsinki), a dual-plate immersion-freezing instrument developed for high-throughput analysis of filter-collected aerosol samples. FrESH uses standard 96-well PCR plates cooled in an ethanol bath with optical detection of freezing.

The relationship between bath temperature (T_{BT}) and droplet temperature (T_{well}) was characterised using five PT100 sensors at fixed temperature and during cooling ramps for two chiller models. Wells were consistently warmer than the bath, and the bath-to-well relationship was approximately linear over the range from 0 to -35 °C, with plate-averaged relations of the form $T_{\mathrm{well}} \approx 0.97\,T_{\mathrm{BT}} + (0.2–0.4)$ °C. Root-mean-square residuals of the plate-averaged linear fits were generally around 0.1 °C and remained below 0.2 °C in the sensor-resolved summaries. Analysis of routine FrESH measurement data revealed persistent spatial freezing patterns across the plates, consistent with spatial temperature variability. Combining the identified sources of uncertainty gives an estimated droplet-temperature uncertainty of 0.43–0.44 °C (1σ) over the operational range. This temperature characterisation is used to assign droplet temperatures and associated uncertainties in FrESH-derived $N_{\mathrm{INP}}(T)$ spectra.

1 Introduction

Ice-nucleating particles (INPs) initiate heterogeneous freezing in supercooled cloud droplets and influence precipitation formation from mixed-phase clouds, cloud lifetime, and cloud radiative properties (Vali, 1971, 2019). Ambient INP concentrations are commonly expressed as a cumulative activation–temperature spectrum $N_{\mathrm{INP}}(T)$, which can vary by several orders of magnitude across environments and seasons (Schneider et al., 2021). Offline immersion-freezing methods based on aerosol collection on filters followed by droplet-freezing analysis are widely used for routine INP measurements, but the resulting spectra depend strongly on how droplet temperature is assigned (Hiranuma et al., 2015; DeMott et al., 2018; Schrod and Bingemer, 2025).

Many immersion-freezing instruments use multi-well plate designs with optical detection of freezing, but they differ in how the samples are cooled, how heat is transferred to the wells, how temperature is controlled (Kunert et al., 2018; David et al., 2019; Miller et al., 2021; Wang et al., 2025; Bazo et al., 2026). Previous studies have shown that the reported bath, block, or

https://doi.org/10.5194/egusphere-2026-3971
Preprint. Discussion started: 20 August 2026

stage temperature can differ systematically from the actual droplet temperature and that spatial temperature variations across the sample holder can influence the inferred freezing spectrum (Beall et al., 2017; Chen et al., 2018; David et al., 2019; Wang et al., 2025; Gratzl et al., 2025; Bazo et al., 2026; Bergner et al., 2026). Characterising these effects is important for accurate uncertainty estimation to improve interpretation and comparison of INP measurements.

FrESH (Freezing Experiment Setup Helsinki) was developed at the Finnish Meteorological Institute for offline INP measurements and was operated routinely to analyse filter-collected aerosol samples. The system uses two clear, non-skirted 96-well PCR plates with cut corner H12 (BRAND, cat. no. 732-2927) immersed in an ethanol bath with optical detection of freezing. In this study, we characterise the relationship between bath and droplet temperature, assess persistent spatial variability across the plates, and determine an operational temperature uncertainty for routine measurements. The analysis combines static equilibrium experiments using PT100 sensors installed in representative well positions, routine FrESH measurement data from over one thousand runs, and dynamic cooling-ramp experiments performed from 0 to -35 °C at 1 °C min^{-1} under the routine measurement configuration.

2 FrESH measurement system

2.1 System overview

FrESH is an immersion-freezing system used to measure the freezing temperature of water droplets containing suspended aerosol particles. The system consists of a thermostat-controlled ethanol bath, a floating frame holding two standard 96-well PCR plates, and a USB camera for optical detection of freezing events (MOKOSE, 3840 x 2160 pixels, fitted with a 5–50 mm manual zoom CS-mount lens). Each plate contains 96 droplets of 50 μL each. During a measurement, the bath is cooled from 0 to -35 °C at 1 °C min^{-1} while backlit images are recorded every 10 s.

Figure 1 shows the FrESH setup and how the PCR wells are positioned in the ethanol bath. Panel (a) shows the ethanol baths and floating frame, panel (b) the dual-plate frame, and panel (c) a cross-section of an individual PCR well. The floating frame maintains a constant immersion depth despite ethanol contraction during cooling. Wells are filled to about half their height, and the ethanol level is adjusted to match the liquid level inside the wells so that only the lower part of each well is submerged. Because thermal coupling depends on this geometry, the plate level is checked before each run to maintain consistent immersion conditions across both plates.

Three Lauda chiller models have been used in FrESH: RK20 during prototyping and RE1050 and RP1845 during routine operation. The present study focuses on the two operational systems, RE1050 and RP1845.

2.2 Sensing and optical detection

Each chiller records the setpoint temperature, the internal bath temperature (T_{BT}), and the temperature from an external PT100 probe placed in the ethanol near the plates. These signals are logged at 1 Hz. Temperature data and images are timestamped independently, and temperatures are assigned to images by matching the corresponding timestamps.

https://doi.org/10.5194/egusphere-2026-3971
Preprint. Discussion started: 20 August 2026

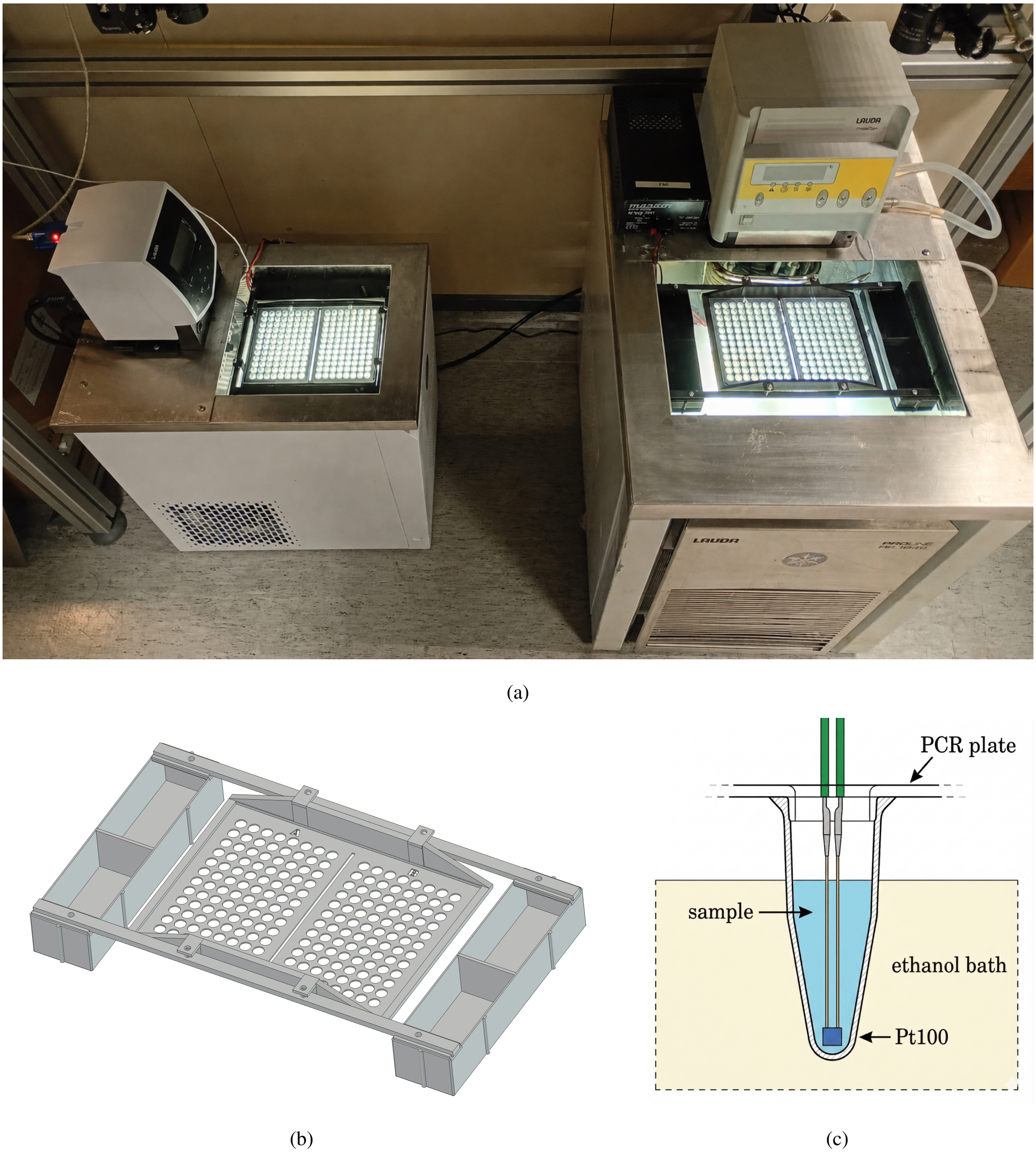

Figure 1. (a) FrESH setup with the two ethanol baths and the floating PCR plate holding frame. (b) CAD view of the dual-plate frame. (c) Cross-section of a PCR well showing sample and ethanol bath level, and PT100 position.

https://doi.org/10.5194/egusphere-2026-3971
Preprint. Discussion started: 20 August 2026

For thermal characterisation, five additional PT100 sensors (Labfacility Ltd, XE-4440-001, thin-film Class A) were installed at representative well positions across the two plates and read using MAX31865 boards connected to a Raspberry Pi. Bath temperature was also verified independently with a calibrated handheld thermometer during separate tests. The sensors were placed to sample both corners and a central region of the plates and to include positions expected to be sensitive to edge-cooling effects: sensor 1 in well H1 of plate A, sensor 2 in well A1 of plate B, sensor 3 in well A12 of plate B, sensor 4 in well H12 of plate A, and sensor 5 in well A6 of plate A.

During image processing, frames are first assigned to the corresponding plate, and well positions are identified in the initial image using a circular Hough transform. The well locations are then tracked through the image sequence by aligning each frame to the initial image. Mean grayscale intensity is calculated for each well to produce a time series, and freezing events are detected as sharp irreversible decreases in transmitted light associated with ice formation. With a cooling rate of 1 °C min^{-1} and an imaging interval of 10 s, the effective temperature resolution is approximately 0.17 °C per frame.

3 Temperature characterisation methods

3.1 Static step experiments

To characterise the relationship between bath and well temperature under near-equilibrium conditions, step experiments were performed from 0 to -35 °C in increments of -5 °C. At each temperature step, the system was allowed to equilibrate for 5–10 min, and the final 2 min of each plateau were averaged to obtain a representative value for each sensor.

The instrumented wells were filled with water to match normal operating conditions. For each sensor i, the bath-to-well relationship was fitted using

$$T_{\mathrm{well},i} = a_i T_{\mathrm{BT}} + b_i.$$

The corresponding offset between well and bath temperature is

$$\Delta T_i = T_{\mathrm{well},i} - T_{\mathrm{BT}} = (a_i - 1) T_{\mathrm{BT}} + b_i.$$

The step experiments were repeated on different days to assess repeatability and to exclude effects from room temperature variations.

3.2 Analysis of position-dependent freezing patterns

Because the five PT100 sensors do not resolve the full temperature structure across the two 96-well plates, routine FrESH measurements were analysed to identify recurring plate-position patterns during operation. This analysis is based on freezing statistics rather than direct temperature measurements and therefore serves only as an empirical indicator of unresolved spatial

https://doi.org/10.5194/egusphere-2026-3971
Preprint. Discussion started: 20 August 2026

heterogeneity. The observed patterns may reflect both temperature differences and other repeatable position-dependent influences, so they are interpreted here as an empirical measure of position-dependent variability rather than as a direct map of well temperature.

For each run k, the freezing temperature of each well $T_i^{(k)}$ was referenced to the median freezing temperature of the corresponding plate in the same run,

$$\delta T_i^{(k)} = T_i^{(k)} - \widetilde{T}_{\text{plate}}^{(k)},$$

with $\widetilde{T}_{\text{plate}}^{(k)}$ the plate median, which was preferred over the plate mean for robustness to occasional anomalous freezing events; replacing it with the mean yields the same spatial pattern. The mean deviation

$$c_i = \frac{1}{M_i} \sum_{k=1}^{M_i} \delta T_i^{(k)}$$

defines a temperature-bias field in °C, where M_i is the number of runs in which well i was used. Spatial autocorrelation of the resulting c_i fields was summarised using Moran's I on the 96-well grid, with neighbouring wells defined by queen connectivity. The field c_i represents the average offset of each well relative to the plate median and quantifies recurring position-dependent differences in apparent freezing temperature.

The spatial maps of c_i are used as diagnostic tools for position-dependent variability that cannot be resolved by the five PT100 sensors. Because c_i combines thermal and non-thermal contributions that cannot be separated from freezing statistics alone, it is used only to define the spatial term in the uncertainty budget, rather than as an operational well-specific correction.

3.3 Dynamic ramp experiments and operational mapping

Dynamic behaviour was characterised during full cooling ramps from 0 to -35 °C at 1 °C min^{-1} with five PT100 sensors installed in representative well positions. These sensors were first characterised against bath temperature in the static step experiments described in Sect. 3.1. The ramp experiments were used to quantify transient differences between bath and well temperature under normal operating conditions and to examine qualitatively whether the dynamic response was consistent with the position-dependent freezing patterns identified in Sect. 3.2.

The operational droplet-temperature estimate used in FrESH is based on a plate-averaged linear relation for each chiller,

$$T_{\text{well,corr}}(t) = a_{\text{chiller}}\, T_{\text{BT}}(t) + b_{\text{chiller}}.$$

Dynamic residuals were computed by matching PT100 and chiller records by timestamp, applying the plate-averaged static bath-to-well correction to the bath temperature at each matched time point, and subtracting the resulting estimate from the simultaneously measured PT100 well temperature.

https://doi.org/10.5194/egusphere-2026-3971
Preprint. Discussion started: 20 August 2026

Table 1. Mean bath-to-well transfer function parameters for the two main FrESH chillers. Values are means and standard deviations across all sensors and runs.

Chiller	a	b (°C)	RMSE (°C)
RE1050	0.974 ± 0.014	0.362 ± 0.170	0.114
RP1845	0.969 ± 0.014	0.192 ± 0.116	0.110

Well-specific corrections are not applied, because the position-dependent field inferred from freezing statistics is not independently constrained and applying it directly at the well level could overfit the historical dataset. Instead, the remaining between-well variability is treated as a contribution to the temperature uncertainty budget. The parameters a_{chiller} and b_{chiller} are plate-averaged for each chiller, and the position-dependent variability not resolved by the five PT100 sensors enters as the term u_{spatial} described in Sect. 4.3. The coherent spatial structure in the heat maps is consistent with bath-scale differences in circulation and heat transfer rather than random well-to-well noise.

4 Results

4.1 Bath-to-well heat transfer

Figure 2 shows the measured bath-to-well temperature offsets for the two main FrESH chillers together with the corresponding plate-averaged linear fits. The step experiments indicate an approximately linear relationship between T_{BT} and well temperature over the full operational range. Across all sensor–chiller combinations, the linear fits yield R^2 values very close to 1, with mean root-mean-square errors of about 0.11 °C. Using plate-averaged parameters averaged across runs and sensors, the correction parameters are a =0.974, b =0.36 °C for RE1050 and a =0.969, b =0.19 °C for RP1845. The fitted parameters are summarised in Table 1. Sensor-resolved parameters and run-to-run standard deviations are provided in Appendix A; these indicate that the fitted transfer functions are stable across repeated experiments, although some sensors show larger variability in intercept than in slope.

Across both chillers, wells remained consistently warmer than T_{BT}, and the offset increased at lower temperatures. At 0 °C, offsets were typically about 0.2–0.5 °C depending on position and chiller, increasing to about 1.1–1.9 °C for RE1050 and 0.8–2.0 °C for RP1845 at -35 °C. RP1845 showed a larger sensor-to-sensor spread at low temperature, with a spread of about 1.23 °C across the five instrumented wells at -35 °C, compared with about 0.79 °C for RE1050. This indicates stronger spatial temperature gradients in RP1845 under static conditions and is consistent with the larger position-dependent variability inferred from the routine-measurement analysis.

4.2 Position-dependent freezing patterns during routine operation

The spatial maps of c_i derived in Sect. 3.2 provide an empirical constraint on position-dependent variability that cannot be resolved by the five PT100 sensors. The resulting fields show clear spatial structure across the plates rather than isolated well-

https://doi.org/10.5194/egusphere-2026-3971
Preprint. Discussion started: 20 August 2026

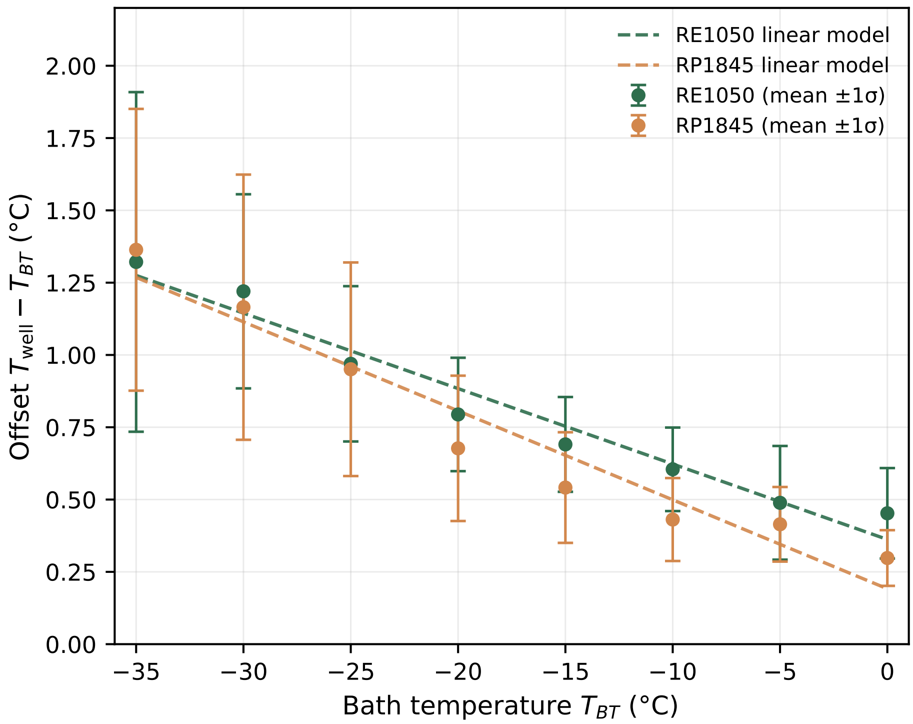

Figure 2. Bath-to-well temperature offset as a function of bath temperature for the two main FrESH chillers. Symbols show the mean offset across sensors and runs in 5 °C temperature step, with error bars indicating $\pm 1\sigma$ across sensors. Dashed lines show the plate-averaged linear relation for each chiller.

to-well noise. Moran's I values were positive for all plates and chillers (RE1050: I =0.69 and 0.78 for plates A and B; RP1845: I =0.68 and 0.73), with permutation-test p <0.001 in all cases, indicating substantial spatial autocorrelation.

The field c_i, computed across all paired runs, shows systematic position-dependent offsets in apparent freezing temperature on the order of 0.5–1 °C relative to the plate median. For RE1050, well-wise mean deviations range from -0.23 to +0.66 °C for plate A and from -0.36 to +0.76 °C for plate B. For RP1845 the values are -0.47 to +0.99 °C for plate A and from -0.37 to +0.70 °C for plate B. These ranges describe the full positional spread of the inferred bias field and are reported here as descriptive spatial amplitudes. In the uncertainty budget, the spatial contribution is instead represented by the weighted standard deviation of c_i, so that all terms entering the combined standard uncertainty are expressed on a consistent sigma basis.

4.3 Dynamic effects and temperature uncertainty budget

The dynamic residuals are smaller than the position-dependent spread inferred from the static and routine-measurement analyses, but they show that a static bath-to-well correction does not fully capture the thermal behaviour of the system during cooling ramps. A dynamic term is therefore included in the operational temperature uncertainty budget.

https://doi.org/10.5194/egusphere-2026-3971
Preprint. Discussion started: 20 August 2026

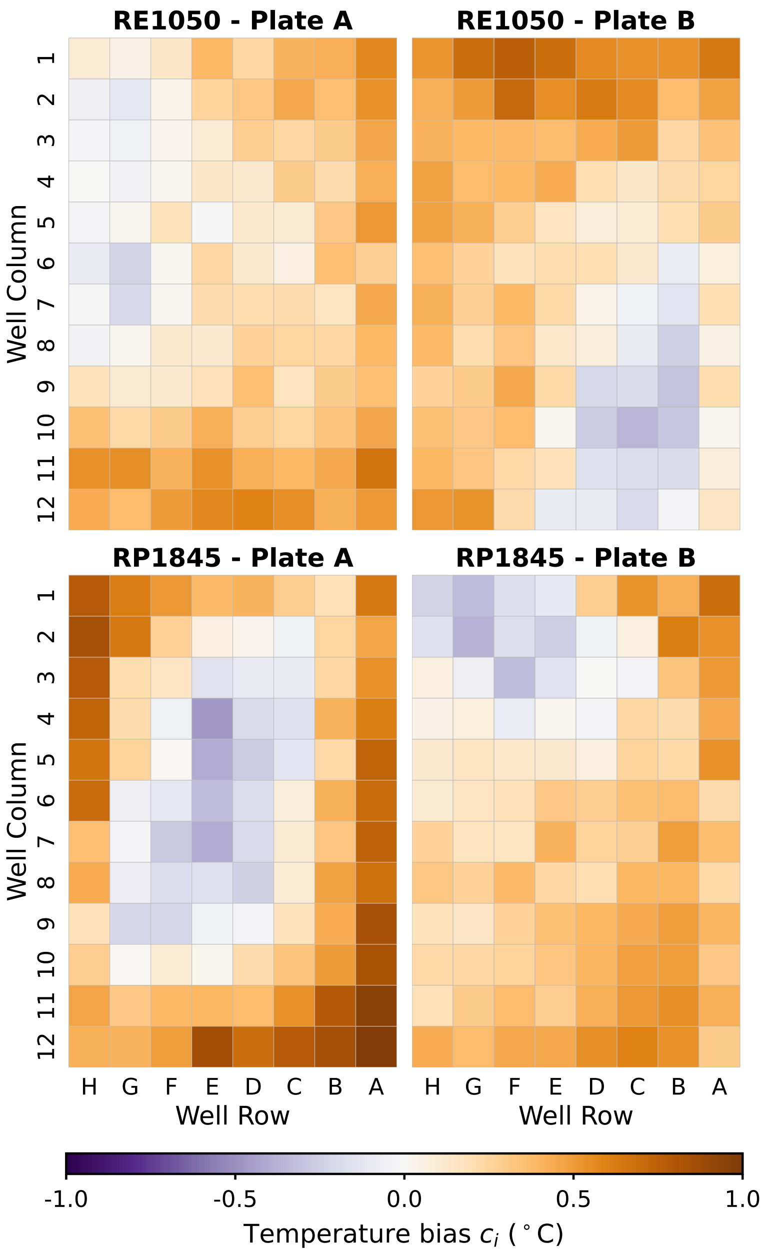

Figure 3. Spatial freezing-temperature bias c_i for the two main FrESH chillers, derived from routine FrESH measurements. Values show the mean deviation of each well from the plate-median freezing temperature.

https://doi.org/10.5194/egusphere-2026-3971
Preprint. Discussion started: 20 August 2026

Ramp experiments show that well temperatures do not follow the imposed cooling exactly. Here, the dynamic residual is defined as the difference between the PT100-measured well temperature during the ramp and the well temperature estimated from the static plate-averaged bath-to-well relation. The residuals are centred close to zero on average for both chillers, but they retain a finite spread, indicating that the static correction does not fully capture the thermal behaviour of the system during continuous cooling. Residuals are generally positive at the beginning of the ramp, consistent with the well remaining slightly warmer than predicted by the static correction during the initial transient, and decrease towards lower temperatures, in some cases becoming weakly negative. This behaviour indicates that the ramp response is not fully described by a single static plate-averaged bath-to-well relation over the full temperature range. The dynamic contribution to uncertainty, u_{dynamic}, is estimated as the mean per-probe standard deviation of these residuals across all runs, which isolates temporal variability from the sensor-to-sensor spread already accounted for in u_{spatial}. This gives 0.32 °C for RE1050 and 0.21 °C for RP1845.

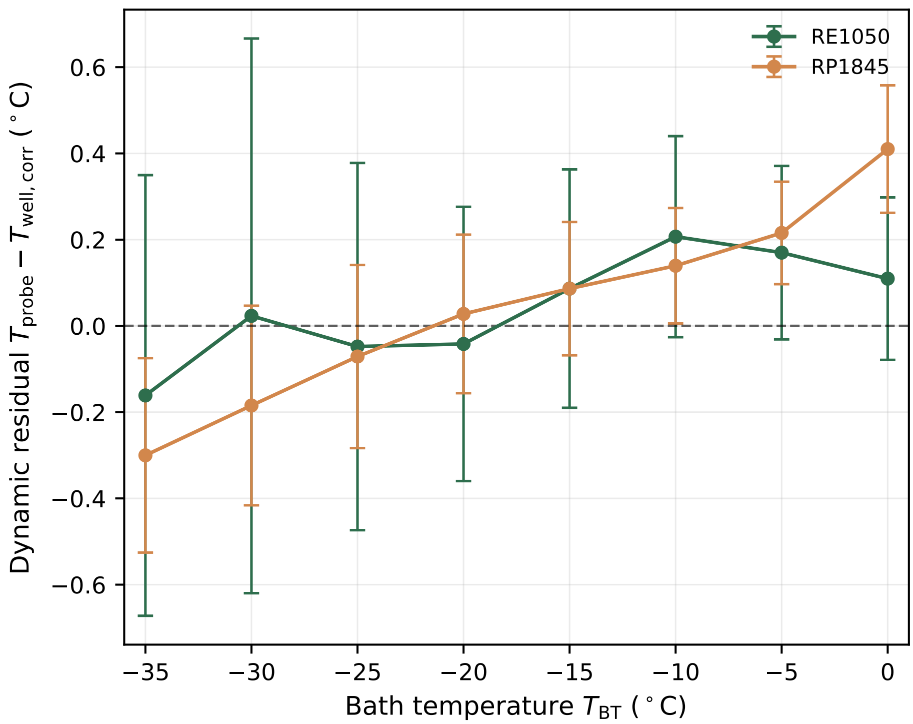

Figure 4. Dynamic temperature residuals during 1 °C min^{-1} cooling ramps after applying the plate-averaged static bath-to-well correction for the two main FrESH chillers (RE1050, RP1845). Symbols show the mean residual $T_{\mathrm{probe}} - T_{\mathrm{well,corr}}$ in 5 °C bath-temperature bins, with error bars indicating $\pm 1\sigma$ of all residual values within each bin. The dashed line marks zero residual.

The FrESH temperature uncertainty budget combines contributions from temporal resolution, bath-probe uncertainty, the residual of the static plate-averaged bath-to-well relation, position-dependent variability, and dynamic effects during cooling ramps. The temporal term associated with 10 s image acquisition at 1 °C min^{-1} is taken as $u_{\mathrm{temporal}} = 0.08$ °C, corresponding

https://doi.org/10.5194/egusphere-2026-3971
Preprint. Discussion started: 20 August 2026

Table 2. Operational temperature uncertainty budget for the two FrESH chillers.

Source	Symbol	RE1050 (°C)	RP1845 (°C)
Temporal	u_{temporal}	0.08	0.08
Bath probe	u_{BT}	0.02	0.02
Model fit	u_{model}	0.11	0.11
Spatial term	u_{spatial}	0.26	0.36
Dynamic	u_{dynamic}	0.32	0.21
Combined	u_T	0.43	0.44

to half of the temperature increment between successive frames and used here as a conservative estimate of timing-related uncertainty in assigned freezing temperature. The bath-probe contribution is u_{BT} =0.02°C, based on the manufacturer-specified accuracy of the bath temperature probe. The static model-fit term, u_{model}, is taken as the mean RMSE of the sensor-resolved linear bath-to-well fits across all runs for each chiller and is 0.11 °C for both RE1050 and RP1845. The spatial term, u_{spatial}, was estimated from the routine-measurement bias field c_i as the weighted standard deviation of the well-mean offsets on each plate, using the number of contributing runs M_i as weights. This gives 0.20 and 0.26 °C for RE1050 and 0.36 and 0.23 °C for RP1845 on plates A and B, respectively. Using the larger plate-specific value for each chiller gives $u_{\text{spatial}} = 0.26$ °C for RE1050 and 0.36 °C for RP1845.

The combined standard uncertainty is 0.43 °C for RE1050 and 0.44 °C for RP1845. The uncertainty is reported here as an operational value for the full measurement range rather than as an explicit function of temperature. The combined uncertainty u_T is calculated by adding the individual contributions in quadrature, treating them as operationally independent contributions to uncertainty in assigned freezing temperature.

5 Discussion

The largest contributions to the FrESH temperature uncertainty arise from spatial variability and dynamic effects during cooling ramps, with their relative importance differing between chillers. Static calibration experiments define the mean bath-to-well relationship for each chiller, and the historical freezing dataset reveals additional spatial variability that could not be resolved by measurements with five PT100 sensors. Together with the ramp experiments, these analyses provide an operational estimate of droplet-temperature assignment uncertainty under routine measurement conditions.

Temperature assignment has a direct impact on derived $N_{\text{INP}}(T)$ spectra. Schrod and Bingemer (2025) showed that uncertainties of ± 0.5 °C can lead to temperature error factors (TEFs) of 1.1–3.2, and that opposite temperature biases between instruments can explain differences commonly observed in intercomparison studies (DeMott et al., 2018, 2025). The uncertainty range reported here ($u_T \approx$ 0.43–0.44 °C, 1σ) is therefore relevant for interpreting $N_{\text{INP}}(T)$ measurements and for comparison with other INP datasets.

https://doi.org/10.5194/egusphere-2026-3971
Preprint. Discussion started: 20 August 2026

Table 3. Reported droplet-level temperature uncertainties or accuracies for selected immersion-freezing instruments from the literature. Values are listed as reported in the respective studies. Because definitions and derivations are not fully uniform across papers, the comparison is indicative rather than strictly one-to-one.

Instrument	Cooling geometry	Reported value (°C)
FrESH (this work)	Ethanol bath	0.43–0.44
FINC (Miller et al., 2021)	Ethanol bath	± 0.5
FINDA-WLU (Wang et al., 2025)	Cold stage	± 0.60
GRAINS (Bazo et al., 2026)	Cold stage	$<$ 0.5
DRINCZ (David et al., 2019)	Ethanol bath	± 0.9
micro-PINGUIN (Wieber et al., 2024)	Gallium bath	± 0.81[a]
TINA (Kunert et al., 2018)	Aluminium block	$<$ 0.2

[a] Reported as accuracy at -10 °C; the same study reports reproducibility of ± 0.20 °C.

Table 3 summarises reported droplet-level temperature uncertainties for selected immersion-freezing instruments. The comparison is intended as context rather than a full review, and the reported values are not directly comparable across studies because they were derived using different methods. FrESH uncertainty falls within the range reported for similar systems.

This work introduces a practical temperature-characterisation and uncertainty-estimation framework that can improve the uncertainty budget of droplet-temperature assignment relative to raw bath temperature readings, without introducing well-specific corrections that are not independently constrained. The calibration and uncertainty framework applies to the current FrESH configuration (96-well plates, 50 μL droplets, partial ethanol immersion, 1 °C min^{-1} cooling rate, and RE1050 and RP1845 chillers); changes in configuration would require re-characterisation of the bath-to-well corrections and spatial bias structure.

6 Conclusions

FrESH shows a stable and approximately linear relationship between bath and well temperature over the operational range from 0 to -35 °C, with wells systematically warmer than the bath. Using bath temperature directly would therefore bias reported freezing temperatures.

The analysis of routine measurements shows spatial differences across the plates, indicating local temperature heterogeneity during routine operation. Because full well-by-well temperature measurements are not available, this effect is treated as an uncertainty contribution rather than corrected explicitly at the well level.

Combining uncertainty contributions from image timing, bath-probe accuracy, the residual of the static plate-averaged bath-to-well relation, position-dependent variability, and dynamic effects during cooling ramps yields an estimated droplet-temperature uncertainty of 0.43 °C (RE1050) and 0.44 °C (RP1845) (1σ) for the FrESH system.

https://doi.org/10.5194/egusphere-2026-3971
Preprint. Discussion started: 20 August 2026

The characterisation presented here is used to assign droplet temperature and associated uncertainty in routine FrESH measurements of $N_{\mathrm{INP}}(T)$ spectra.

Code availability. The analysis scripts used in this study are available at https://doi.org/10.57707/fmi-b2share.zf2e1-9nd11.

Data availability. The datasets supporting this study are available at https://doi.org/10.57707/fmi-b2share.zf2e1-9nd11. These include the static step-experiment summaries, anonymised pooled freezing-temperature data from routine FrESH measurements, and dynamic ramp residual data used in the analyses presented here.

Author contributions. GPF carried out the experiments, processed the data, performed the analysis, and prepared the manuscript. AW contributed to the study design, interpretation of the results, and revision of the manuscript.

Competing interests. The authors declare that they have no conflict of interest.

Acknowledgements. We acknowledge the support of the Academy of Finland (grant numbers 342227 and 337552) and personal funding from the Vilho, Yrjö and Kalle Väisälä Foundation of the Finnish Academy of Science and Letters.

An AI-based tool was used for limited support in code drafting and language editing during manuscript preparation. All analysis code, results, interpretations, and final text were reviewed and validated by the authors.

Appendix A: FrESH calibration parameters

Table A1 summarises the bath-to-well relation parameters for each instrumented PT100 position and chiller, including mean values across all valid step runs and the corresponding run-to-run standard deviations.

https://doi.org/10.5194/egusphere-2026-3971
Preprint. Discussion started: 20 August 2026

Table A1. Sensor-resolved bath-to-well transfer function parameters for the two main FrESH chillers. Values are means and standard deviations across repeated step experiments.

		a		b (°C)		RMSE (°C)		R^2	n runs
Chiller	Sensor	mean	std	mean	std	mean	std	mean	
RE1050	Sensor 1	0.973	0.004	0.298	0.128	0.089	0.029	1.000	6
RE1050	Sensor 2	0.974	0.017	0.353	0.091	0.111	0.027	1.000	6
RE1050	Sensor 3	0.961	0.020	0.304	0.266	0.193	0.090	1.000	6
RE1050	Sensor 4	0.979	0.005	0.376	0.181	0.078	0.020	1.000	6
RE1050	Sensor 5	0.984	0.009	0.479	0.117	0.096	0.009	1.000	6
RP1845	Sensor 1	0.950	0.005	0.090	0.047	0.170	0.045	1.000	6
RP1845	Sensor 2	0.984	0.003	0.193	0.048	0.058	0.016	1.000	6
RP1845	Sensor 3	0.980	0.006	0.131	0.091	0.088	0.037	1.000	6
RP1845	Sensor 4	0.959	0.009	0.184	0.083	0.143	0.040	1.000	6
RP1845	Sensor 5	0.973	0.004	0.360	0.089	0.090	0.031	1.000	6

https://doi.org/10.5194/egusphere-2026-3971
Preprint. Discussion started: 20 August 2026

References

Bazo, E., Ruiz-Galera, O., Alados-Arboledas, L., Böhmländer, A., Höhler, K., Kim, N., Lacher, L., Möhler, O., Olmo, F. J., Perez Fogwill, G., Piedehierro, A. A., Umo, N. S., Welti, A., Titos, G., and Cazorla, A.: Evaluation of different sampling methods to determine the ice-nucleating particle concentration in the atmosphere using the GRAnada Ice Nuclei Spectrometer (GRAINS), Atmospheric Measurement Techniques, 19, 2695–2713, https://doi.org/10.5194/amt-19-2695-2026, 2026.

Beall, C. M., Stokes, M. D., Hill, T. C., DeMott, P. J., DeWald, J. T., and Prather, K. A.: Automation and heat transfer characterization of immersion mode spectroscopy for analysis of ice nucleating particles, Atmospheric Measurement Techniques, 10, 2613–2626, https://doi.org/10.5194/amt-10-2613-2017, 2017.

Bergner, N., Marsh, G., Barry, K., Lacher, L., Böhmländer, A., Alden, J., Ahlqvist, C., Altshuler, I., Bröder, L., Farinotti, D., Favre, L., Guillosson, C., Heutte, B., Höhler, K., Pohorsky, R., Weng, J., and Schmale, J.: Ice-nucleating particles in Greenlandic glacial outwash plains, EGUsphere, https://doi.org/10.5194/egusphere-2026-484, 2026.

Chen, J., Pei, X., Wang, H., Chen, J., Zhu, Y., Tang, M., and Wu, Z.: Development, Characterization, and Validation of a Cold Stage-Based Ice Nucleation Array (PKU-INA), Atmosphere, 9, 357, https://doi.org/10.3390/atmos9090357, 2018.

David, R. O., Cascajo-Castresana, M., Brennan, K. P., Rösch, M., Els, N., Werz, J., Weichlinger, V., Boynton, L. S., Bogler, S., Borduas-Dedekind, N., Marcolli, C., and Kanji, Z. A.: Development of the DRoplet Ice Nuclei Counter Zurich (DRINCZ): validation and application to field-collected snow samples, Atmospheric Measurement Techniques, 12, 6865–6888, https://doi.org/10.5194/amt-12-6865-2019, 2019.

DeMott, P. J., Möhler, O., Cziczo, D. J., Hiranuma, N., Petters, M. D., Petters, S. S., Belosi, F., Bingemer, H. G., Brooks, S. D., Budke, C., Burkert-Kohn, M., Collier, K. N., Danielczok, A., Eppers, O., Felgitsch, L., Garimella, S., Grothe, H., Herenz, P., Hill, T. C. J., Höhler, K., Kanji, Z. A., Kiselev, A., Koop, T., Kristensen, T. B., Krüger, K., Kulkarni, G., Levin, E. J. T., Murray, B. J., Nicosia, A., O'Sullivan, D., Peckhaus, A., Polen, M. J., Price, H. C., Reicher, N., Rothenberg, D. A., Rudich, Y., Santachiara, G., Schiebel, T., Schrod, J., Seifried, T. M., Stratmann, F., Sullivan, R. C., Suski, K. J., Szakáll, M., Taylor, H. P., Ullrich, R., Vergara-Temprado, J., Wagner, R., Whale, T. F., Weber, D., Welti, A., Wilson, T. W., Wolf, M. J., and Zenker, J.: The Fifth International Workshop on Ice Nucleation phase 2 (FIN-02): laboratory intercomparison of ice nucleation measurements, Atmospheric Measurement Techniques, 11, 6231–6257, https://doi.org/10.5194/amt-11-6231-2018, 2018.

DeMott, P. J., Mirrielees, J. A., Petters, S. S., Cziczo, D. J., Petters, M. D., Bingemer, H. G., Hill, T. C. J., Froyd, K., Garimella, S., Hallar, A. G., Levin, E. J. T., McCubbin, I. B., Perring, A. E., Rapp, C. N., Schiebel, T., Schrod, J., Suski, K. J., Weber, D., Wolf, M. J., Zawadowicz, M., Zenker, J., Möhler, O., and Brooks, S. D.: Field intercomparison of ice nucleation measurements: the Fifth International Workshop on Ice Nucleation Phase 3 (FIN-03), Atmospheric Measurement Techniques, 18, 639–672, https://doi.org/10.5194/amt-18-639-2025, 2025.

Gratzl, J., Böhmländer, A., Pätsi, S., Pogner, C.-E., Gorfer, M., Brus, D., Doulgeris, K. M., Wieland, F., Asmi, E., Saarto, A., Möhler, O., Stolzenburg, D., and Grothe, H.: Locally emitted fungal spores serve as high-temperature ice nucleating particles in the European sub-Arctic, Atmospheric Chemistry and Physics, 25, 12 007–12 035, https://doi.org/10.5194/acp-25-12007-2025, 2025.

Hiranuma, N., Augustin-Bauditz, S., Bingemer, H., Budke, C., Curtius, J., Danielczok, A., Diehl, K., Dreischmeier, K., Ebert, M., Frank, F., Hoffmann, N., Kandler, K., Kiselev, A., Koop, T., Leisner, T., Möhler, O., Nillius, B., Peckhaus, A., Rose, D., Weinbruch, S., Wex, H., Boose, Y., DeMott, P. J., Hader, J. D., Hill, T. C. J., Kanji, Z. A., Kulkarni, G., Levin, E. J. T., McCluskey, C. S., Murakami, M., Murray, B. J., Niedermeier, D., Petters, M. D., O'Sullivan, D., Saito, A., Schill, G. P., Tajiri, T., Tolbert, M. A., Welti, A., Whale, T. F., Wright,

https://doi.org/10.5194/egusphere-2026-3971
Preprint. Discussion started: 20 August 2026

T. P., and Yamashita, K.: A comprehensive laboratory study on the immersion freezing behavior of illite NX particles: a comparison of 17 ice nucleation measurement techniques, Atmospheric Chemistry and Physics, 15, 2489–2518, https://doi.org/10.5194/acp-15-2489-2015, 2015.

Kunert, A. T., Lamneck, M., Helleis, F., Pöschl, U., Pöhlker, M. L., and Fröhlich-Nowoisky, J.: Twin-plate Ice Nucleation Assay (TINA) with infrared detection for high-throughput droplet freezing experiments with biological ice nuclei in laboratory and field samples, Atmospheric Measurement Techniques, 11, 6327–6337, https://doi.org/10.5194/amt-11-6327-2018, 2018.

Miller, A. J., Brennan, K. P., Mignani, C., Wieder, J., David, R. O., and Borduas-Dedekind, N.: Development of the drop Freezing Ice Nuclei Counter (FINC), intercomparison of droplet freezing techniques, and use of soluble lignin as an atmospheric ice nucleation standard, Atmospheric Measurement Techniques, 14, 3131–3151, https://doi.org/10.5194/amt-14-3131-2021, 2021.

Schneider, J., Höhler, K., Heikkilä, P., Keskinen, J., Bertozzi, B., Bogert, P., Schorr, T., Umo, N. S., Vogel, F., Brasseur, Z., Wu, Y., Hakala, S., Duplissy, J., Moisseev, D., Kulmala, M., Adams, M. P., Murray, B. J., Korhonen, K., Hao, L., Thomson, E. S., Castarède, D., Leisner, T., Petäjä, T., and Möhler, O.: The seasonal cycle of ice-nucleating particles linked to the abundance of biogenic aerosol in boreal forests, Atmospheric Chemistry and Physics, 21, 3899–3918, https://doi.org/10.5194/acp-21-3899-2021, 2021.

Schrod, J. and Bingemer, H. G.: A view on recent ice-nucleating particle intercomparison studies: why the uncertainty of the activation temperature matters, Atmospheric Measurement Techniques, 18, 2591–2605, https://doi.org/10.5194/amt-18-2591-2025, 2025.

Vali, G.: Quantitative Evaluation of Experimental Results on the Heterogeneous Freezing Nucleation of Supercooled Liquids, Journal of the Atmospheric Sciences, 28, 402–409, https://doi.org/10.1175/1520-0469(1971)028<0402:QEOERA>2.0.CO;2, 1971.

Vali, G.: Revisiting the differential freezing nucleus spectra derived from drop-freezing experiments: methods of calculation, applications, and confidence limits, Atmospheric Measurement Techniques, 12, 1219–1231, https://doi.org/10.5194/amt-12-1219-2019, 2019.

Wang, K., Bi, K., Chen, S., Hartmann, M., Wu, Z., Gao, J., Xu, X., Cheng, Y., Huang, M., Chen, Y., Xue, H., Wang, B., Hu, Y., Zhang, X., Ma, X., Li, R., Tian, P., Möhler, O., Wex, H., Stratmann, F., Chen, J., and Gong, X.: An improved Freezing Ice Nucleation Detection Analyzer (FINDA) for droplet immersion freezing measurement, Atmospheric Measurement Techniques, 18, 5823–5840, https://doi.org/10.5194/amt-18-5823-2025, 2025.

Wieber, C., Rosenhøj Jeppesen, M., Finster, K., Melvad, C., and Šantl Temkiv, T.: Micro-PINGUIN: microtiter-plate-based instrument for ice nucleation detection in gallium with an infrared camera, Atmospheric Measurement Techniques, 17, 2707–2719, https://doi.org/10.5194/amt-17-2707-2024, 2024.